

The High-Cut Parameter (Kappa) for the Near-Surface Geology in and around the Taipei Basin, Taiwan

by Ming-Wey Huang, Kuo-Liang Wen, Shun-Chiang Chang, Chi-Ling Chang, Sheu-Yien Liu, and Kuei-Pao Chen

Abstract The decay parameter at the high frequency (kappa value, κ) introduced by Anderson and Hough (1984) is measured from 54 stations situated in and around the Taipei basin, northern Taiwan. Different frequency windows for the *S*-wave amplitude spectra are used to measure the κ_r value for each individual record. The preferred κ_r values are determined by the least-squared fitting with the best correlation coefficient. The site-specific κ_0 values, which are computed by removing the anelastic effect of regional geological structure by grouping κ_r into the crustal and subduction events according to the focal depth and site classification (i.e., class B, C, D, and E sites), are calculated to be in the range of 0.034–0.066 s. We correlate the κ_0 values with the averaged shear-wave velocity of the topmost 30-m layer V_{S30} and find the independence of κ_0 on V_{S30} . In addition, 28 stations lie on sediment in the Taipei basin. The gradient of κ_0 versus the sedimentary thickness to the Tertiary base in the basin is calculated, and then used to estimate the effective quality factor Q_{ef} of the layer. Q_{ef} is 75.3 for the whole sedimentary layers (above the Tertiary base). Given one standard deviation, Q_{ef} are in the 41.9–376.7 range. Q_{ef} can provide an accurate referred parameter for the future ground-motion simulation applications.

Introduction

A filtered/high-cut parameter (kappa) at the high frequency was first introduced by Anderson and Hough (1984), namely the kappa value, denoted by κ , which characterizes the behavior of spectrum decay with frequency for the shear waves due to the effect of several kilometers depth from surface. Common applications for κ are focused on the engineering seismology that has been suggested to be an important input of simulation of ground motion based on the stochastic model (Boore, 1983, 1996, 2003), a shape controller at high frequencies on the site amplification function for different site conditions (Boore and Joyner, 1997; Sokolov *et al.*, 2004; Huang *et al.*, 2005, 2007, 2009), and even as an adjustment factor taken into evaluation on ground-motion prediction equations (GMPes; Scherbaum *et al.*, 2006; Van Houtte *et al.*, 2011). A recent summary review of κ on the applications and restrictions is found in the study of Ktenidou *et al.* (2014).

In general, the spectral amplitude of acceleration recordings decays exponentially with frequency $\sim A_0 e^{-\pi\kappa r f}$, in which A_0 are the spectral amplitudes and f is the frequency. The κ_r value can be directly measured by a linear fit on the spectra amplitudes in semilogarithmic scale at a frequency greater than a specific frequency f_e . The slope of linear fit is $-\pi\kappa_r$. The κ_r values are obtained from individual records of any epicentral distance. Anderson and Hough (1984) also concluded the terms of the distance-corrected value κ_r and the site-dependent

value κ_0 from the measured κ_r values for the individual site. The κ_r value represents the anelastic effect of regional geological structure assuming the dependency on distance between a site and the epicenter. Anderson and Hough (1984) and Anderson (1991) defined the distance- and site-dependent κ_r value in the form of $\kappa_r = \kappa_0 + \kappa(r)$, in which $\kappa(r)$ is formulated as $m \times R_e$ under assumption of dependency on the epicentral distance (R_e). The κ_0 value is generally considered to vary with the site conditions whereas the seismic waves propagate through the near-subsurface geology. The intercept also means the zero-distance κ_r value; that is, a representative of a site. We decompose the measured κ_r value to obtain the site-specific κ_0 for comparison with the site indicator in a later section. The physics of the κ_r value is not completely understood and is still debated. Studies attribute it as source dependency (Papageorgiou and Aki, 1983; Purvance and Anderson, 2003); others support it as site dependency (Anderson and Hough, 1984; Anderson, 1991). In this study, we follow the assumption of Anderson and Hough (1984) to continue the investigation of κ_r on site dependence.

Parolai and Bindi (2004) analyzed the effect of soil layer on the estimate of κ_r value and concluded that the fundamental resonance frequency and even the first-mode frequency of harmonics would cause discrepancy between the measured κ_r value and its original one. They also mention that the

wider spectral windows applied to estimate the κ_r value would reduce or average out the effect of local peaks that would bias the measured results to be more or less.

The aims of this study are to correlate the site-specific κ_0 value to the existing site indicator; that is, the averaged shear velocity of the topmost 30-m layer V_{S30} , and to evaluate the effective Q value of the sedimentary layers in the Taipei basin. Prior to correlation and evaluation, more stable and precise κ_r values for each individual record are measured under the process of least-squared fitting with varied frequency windows on spectral amplitudes for the shear wave and are determined by the correlation coefficient with the best result. The selected window of frequency on fitting the spectral amplitudes is subjective (Ktenidou *et al.*, 2013). To reduce the visual and manual errors on the spectral amplitudes, there are studies on selecting the start and stop of frequencies varied in the 1–20 and 11–70 Hz ranges, respectively, to minimize the fitting errors in obtaining the κ_r values (Ktenidou *et al.*, 2013; Edwards *et al.*, 2015). We follow and modify the conception of methodology on selecting frequency windows to obtain κ_r .

The near-surface V_{S30} are commonly used to identify the site conditions under National Earthquake Hazards Reduction Program (NEHRP); that is, classes A, B, C, D, and E representing hard rock, rock, very dense soil and soft rock, stiff soils, and soft soils, respectively (Building Seismic Safety Council [BSSC], 2001; Boore, 2004; Holzer *et al.*, 2005). We do a comparison of the κ_0 – V_{S30} couples in this study to those of relationships developed in other areas (Chandler *et al.*, 2006; Edwards *et al.*, 2011; Van Houtte *et al.*, 2011; Ktenidou *et al.*, 2015). In addition, the thickness to the known basement for each observation site was suggested to be related to κ_0 (Campbell, 2009; Ktenidou *et al.*, 2015). We apply procedures to correlate κ_0 with thickness to the base rock, as well as the thickness of the topmost soil layer to infer the effective Q values for the future applications on the simulations of ground motion. Finally, κ_0 correlates to dominant/resonant frequency measured from microtremor arrays deployed inside the Taipei basin.

Recording Sites and Data

The data are from the Geophysical Database Management System (GDMS; Shin *et al.*, 2013), an integrated information system regarding the geophysical observation in Taiwan area, developed by the Central Weather Bureau (CWB), Taiwan. The observation stations in GDMS belong to the network of the Taiwan Strong Motion Instrumentation Program (TSMIP), which has recorded the strong ground motions at free field since 1992. The details regarding the network can be found in Liu *et al.* (1999). Each station is equipped with triaxial force-balanced accelerometers, with a flat frequency response from direct current to about 50.0 Hz. The seismograms of acceleration are selected from the period of 1993 to 2010 with local magnitude (M_L) ranging from 5.0 to 7.3 and focal depths in the 1.9–175.6 km range. The M_L is determined using accelerograms to simulate the Wood–

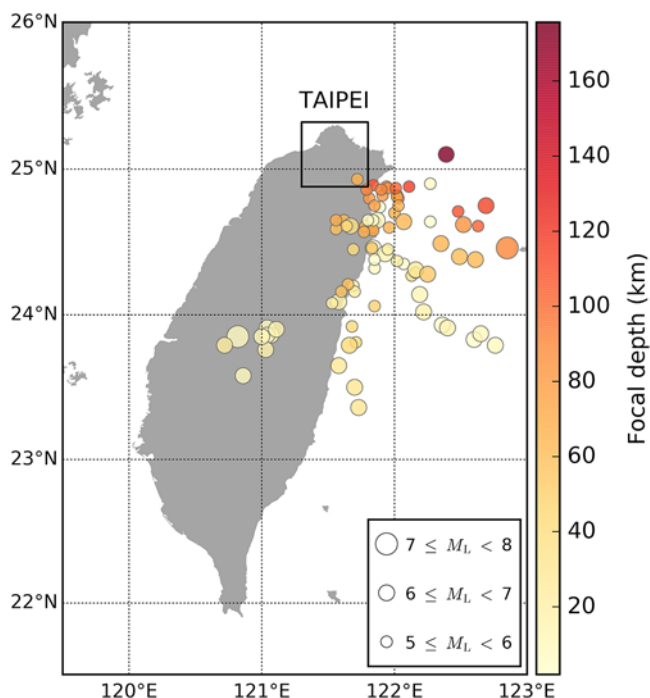


Figure 1. The distribution of earthquakes in three sizes of circles indicates the earthquake magnitude over the period of 1993 to 2010. The rectangle shows the location of the Taipei basin. The color version of this figure is available only in the electronic edition.

Anderson seismograms (Shin, 1993). The total number of events and records for analysis at 54 stations are 85 and 1267, respectively. Figure 1 shows the distribution of the earthquakes, with three sizes of circles displaying the various magnitudes and colors indicating the focal depths.

The stations of TSMIP network are installed in and around the Taipei basin, where the geographical environment is surrounded by Tatun volcanoes in the north, Linkou Tableland in the east, and the western foothill in the southeast (SE), as shown in Figure 2a. The geological sediments in the basin can be recognized by four layers; that is, (from top to bottom) Sungshan Formation, Chingmei Formation, Wuku Formation, and Banchiao Formation, over a base rock of the Tertiary from shallow seismic reflection surveys and borehole-drilling data (Wang *et al.*, 1996, 2004; Fig. 2b). The topmost Sungshan Formation is composed of unconsolidated sand, silt, and clay and is attributed to the lowest S -wave velocity of 170, 230, and 340 m/s. The averaged S -wave velocities are 450, 660, and 880 m/s, respectively, for the Chingmei Formation, Wuku Formation, and Banchiao Formation. Many studies show significant site effect induced by the geology and topography beneath the basin from analysis of seismic data (Wen *et al.*, 1995; Wen and Peng, 1998; Wang *et al.*, 2004; Sokolov *et al.*, 2009). The first analysis of downhole array on site amplification in the Taipei basin was given by Wen *et al.* (1995), which concluded that the larger amplification of peak ground acceleration (PGA) 60 m depth is due to the soft-soil layer. Although Wang *et al.* (2004) compared the PGAs of 50

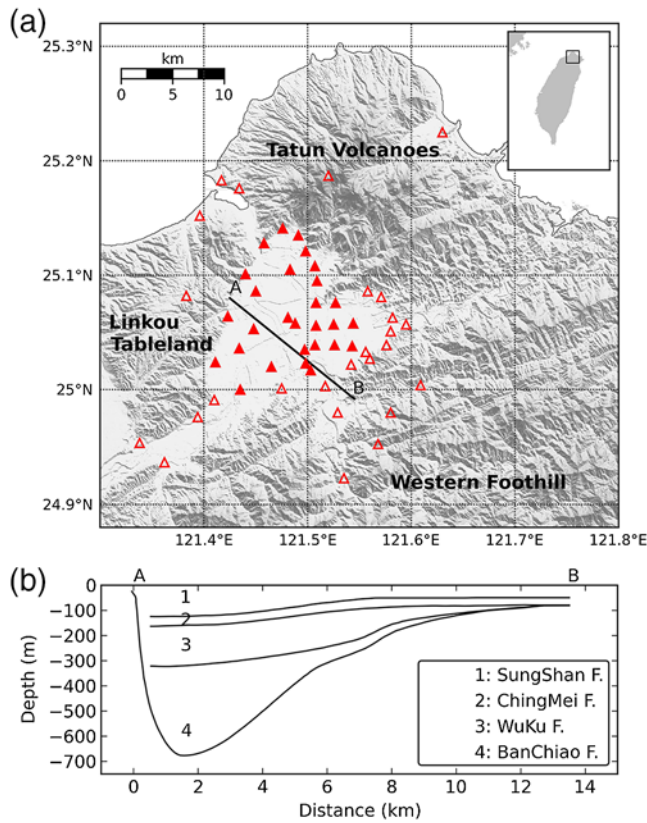


Figure 2. (a) The distribution of stations in use to evaluate the kappa value. The solid triangles display the stations located above the Tertiary base rock. (b) The geological cross section of Taipei basin along northwest–southeast direction above the Tertiary base rock after Wang *et al.* (2004). The color version of this figure is available only in the electronic edition.

earthquakes in the Taipei basin with the S -wave velocity structures, results showed high PGAs correlated with low S -wave velocity. Wen and Peng (1998) analyzed the amplitude spectral ratio of TSMIP's seismic data in the Taipei basin. The frequency bands of 0.2–1.0 Hz are correlated with the bathymetry of Tertiary base rock, leading to an amplification factor of at least 1.5. Sokolov *et al.* (2009) characterized the large site amplification at frequencies 0.3–1.0 Hz inside the basin. Furthermore, seismic-wave propagation simulations based on the structure of seismic-wave velocity can show the amplifications of PGA to be a factor of 5 (Lee *et al.*, 2008). In addition, Miksat *et al.* (2010) give a maximum factor of 8 from ground simulations related to the rock site based on the structure of seismic-wave velocity. The basin tectonics can trap the seismic energy and amplify the seismic waves that can be found from the spectral analysis of seismograms or from waveform simulations. Figure 2a shows the study area and the distribution of stations denoted by open and solid triangles. The solid triangles display the stations located inside the Taipei basin. As shown in Figure 3, the gray area is the subsurface topography of the Tertiary base rock, which tilts from east to west in depth distance span of about 13 km and reaches the deepest depth of ~ 750 m at the northwest (NW) of the basin. The notes A and

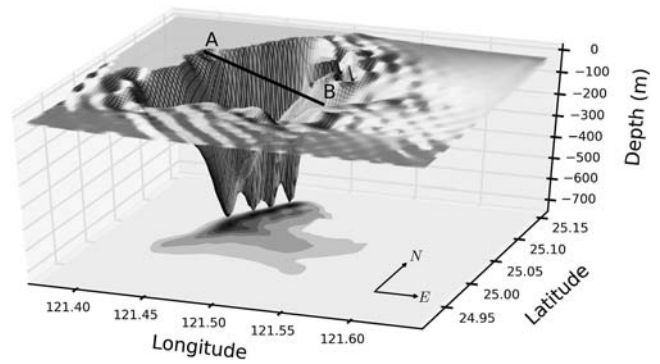


Figure 3. The subsurface topography of the Tertiary base rock underneath the Taipei basin tilted from east to west to a maximum depth of about 750 m after Wang *et al.* (2004).

B correspond to those in Figure 2a. The details of the stations are listed in Table 1, in which D_B is the thickness of the sediment above the Tertiary base rock. The M_L versus R_e and focal depths, respectively, are shown in Figure 4. The R_e ranges from 18.6 to 205.0 km. Seismograms are from both the crustal and subduction events.

Method

Estimate of κ_r Value

The study of Anderson and Hough (1984) defined the decay shape for the Fourier spectra of S wave $A(f)$ with frequencies greater than a specific one f_e , which is definitive after the corner frequency f_c , in the form of

$$A(f) = A_0 e^{-\pi \kappa_r f}, f > f_e. \quad (1)$$

The κ_r value is the decay parameter in second. This equation can be expressed as the overall and frequency-independent attenuation within a chosen range of frequencies under assumption. The slope of equation (1) can be obtained from the fit on the semilogarithmic plot of spectral amplitudes over a certain window of frequencies starting at f_e and stopping before the spectra of the background noise or the flat response of instrument.

Two steps are adopted to measure the κ_r values from the seismic records. The first step is that the S wave of recordings for the horizontal components are computed from waveform in time series to the frequency spectra. To speed up the computation based on the technique of fast Fourier transformation, two time windows are selected for comparison after manually picking the arrival of P and S waves. The length of S -wave window for $M_L > 5.0$ in Taiwan can be obtained using Lee *et al.* (2015). The strong-shaking duration, which is commonly considered as the S -wave time window, is in terms of earthquake magnitude (associated with f_c), distance from source, and site condition (V_{S30}). We denote the time windows w_1 and w_2 as the pre- P - and S -wave time windows, respectively. The w_1 can be considered as background noise and is equal to the length of w_2 . Figures 5a and 5b display the waveform of the north–south (N–S) component and those of the

Table 1
Station's Parameters Used in This Study

| Station | Longitude (°) | Latitude (°) | Site Class | V_{S30} (m/s) | Thickness, D_B (m) | κ_0 (s) | $\sigma(\kappa_0)$ (s) |
|---------|---------------|--------------|------------|-----------------|----------------------|----------------|------------------------|
| TAP001 | 121.507 | 25.039 | E | 160.1 | 207.3 | 0.036 | 0.018 |
| TAP002 | 121.458 | 25.128 | C | 374.0 | — | 0.055 | 0.013 |
| TAP003 | 121.450 | 25.086 | D | 209.4 | 579.1 | 0.063 | 0.016 |
| TAP004 | 121.483 | 25.105 | D | 195.5 | 315.0 | 0.050 | 0.007 |
| TAP005 | 121.507 | 25.108 | E | 177.0 | 116.4 | 0.041 | 0.014 |
| TAP006 | 121.509 | 25.095 | D | 198.4 | 154.9 | 0.061 | 0.008 |
| TAP007 | 121.508 | 25.076 | D | 204.3 | 66.0 | 0.053 | 0.011 |
| TAP008 | 121.527 | 25.076 | D | 191.6 | 49.0 | 0.057 | 0.015 |
| TAP009 | 121.571 | 25.081 | D | 187.6 | — | 0.039 | 0.014 |
| TAP010 | 121.481 | 25.063 | D | 217.5 | 276.8 | 0.063 | 0.013 |
| TAP011 | 121.488 | 25.058 | D | 211.1 | 252.0 | 0.061 | 0.014 |
| TAP012 | 121.508 | 25.056 | D | 207.4 | 200.7 | 0.057 | 0.008 |
| TAP013 | 121.525 | 25.057 | D | 207.9 | 158.1 | 0.063 | 0.012 |
| TAP014 | 121.544 | 25.058 | D | 192.1 | 106.4 | 0.066 | 0.012 |
| TAP015 | 121.580 | 25.051 | D | 208.1 | — | 0.043 | 0.010 |
| TAP016 | 121.423 | 25.064 | D | 326.6 | 50.5 | 0.045 | 0.015 |
| TAP017 | 121.448 | 25.053 | D | 221.4 | 463.8 | 0.046 | 0.015 |
| TAP019 | 121.497 | 25.035 | D | 225.2 | 207.7 | 0.052 | 0.012 |
| TAP020 | 121.526 | 25.039 | D | 224.2 | 165.4 | 0.062 | 0.011 |
| TAP021 | 121.543 | 25.038 | E | 165.3 | 110.4 | 0.064 | 0.012 |
| TAP022 | 121.556 | 25.033 | D | 181.0 | — | 0.058 | 0.018 |
| TAP024 | 121.465 | 25.020 | D | 187.8 | 160.2 | 0.046 | 0.014 |
| TAP025 | 121.498 | 25.023 | D | 250.2 | 191.8 | 0.060 | 0.012 |
| TAP026 | 121.503 | 25.017 | D | 200.6 | 156.8 | 0.061 | 0.011 |
| TAP027 | 121.517 | 25.003 | D | 195.7 | — | 0.057 | 0.008 |
| TAP031 | 121.542 | 25.022 | D | 222.0 | — | 0.060 | 0.012 |
| TAP032 | 121.475 | 25.001 | D | 314.9 | — | 0.051 | 0.011 |
| TAP033 | 121.529 | 24.980 | C | 486.3 | — | 0.040 | 0.014 |
| TAP035 | 121.535 | 24.923 | C | 404.7 | — | 0.058 | 0.006 |
| TAP037 | 121.434 | 25.036 | D | 219.9 | 311.5 | 0.057 | 0.008 |
| TAP038 | 121.411 | 25.024 | D | 209.0 | 128.8 | 0.059 | 0.013 |
| TAP039 | 121.362 | 24.937 | C | 661.6 | — | 0.034 | 0.005 |
| TAP040 | 121.434 | 25.176 | C | 432.5 | — | 0.050 | 0.012 |
| TAP041 | 121.417 | 25.183 | C | 360.5 | — | 0.050 | 0.009 |
| TAP043 | 121.410 | 24.991 | C | 382.6 | — | 0.051 | 0.008 |
| TAP044 | 121.394 | 24.976 | C | 473.0 | — | 0.052 | 0.009 |
| TAP047 | 121.338 | 24.954 | C | 571.2 | — | 0.045 | 0.007 |
| TAP050 | 121.396 | 25.152 | D | 280.7 | — | 0.058 | 0.010 |
| TAP051 | 121.440 | 25.101 | C | 401.8 | 55.8 | 0.042 | 0.011 |
| TAP052 | 121.383 | 25.082 | C | 434.4 | — | 0.047 | 0.012 |
| TAP054 | 121.435 | 25.000 | D | 309.7 | 113.9 | 0.051 | 0.006 |
| TAP066 | 121.520 | 25.187 | C | 658.0 | — | 0.059 | 0.016 |
| TAP067 | 121.580 | 24.980 | B | 815.0 | — | 0.050 | 0.008 |
| TAP071 | 121.609 | 25.004 | B | 831.4 | — | 0.049 | 0.012 |
| TAP084 | 121.630 | 25.225 | D | 204.1 | — | 0.047 | 0.012 |
| TAP086 | 121.568 | 24.953 | B | 942.8 | — | 0.050 | 0.008 |
| TAP088 | 121.576 | 25.039 | D | 228.0 | — | 0.062 | 0.014 |
| TAP089 | 121.560 | 25.027 | C | 442.1 | — | 0.054 | 0.009 |
| TAP090 | 121.595 | 25.057 | D | 324.6 | — | 0.044 | 0.013 |
| TAP091 | 121.582 | 25.063 | E | 177.3 | — | 0.050 | 0.010 |
| TAP093 | 121.558 | 25.086 | D | 193.6 | — | 0.054 | 0.012 |
| TAP094 | 121.476 | 25.141 | C | 409.9 | 142.3 | 0.047 | 0.010 |
| TAP095 | 121.491 | 25.135 | D | 205.9 | 65.7 | 0.043 | 0.013 |
| TAP096 | 121.498 | 25.121 | E | 161.0 | 110.7 | 0.046 | 0.012 |

Site classes and V_{S30} after Kuo *et al.* (2012); V_{S30} , the averaged S -wave velocity of the topmost 30 m layer; the thickness for the whole sediment (D_B) above the Tertiary base rock; dash indicates that data are not available.

east–west (E–W) component, respectively. The gray lines show the pre- P - and S -wave windows regarding w1 and w2. The time series were processed using a cosine taper of 5% at both ends of the windows. The dark and gray lines in Fig-

ure 5c,d show the smoothed spectral amplitudes of pre- P and S waves for the time windows (i.e., w1 and w2). In Figure 5c, d, the spectral amplitudes of w2 (less than 23 Hz) are larger than those of w1, which is due to more spectral amplitude of

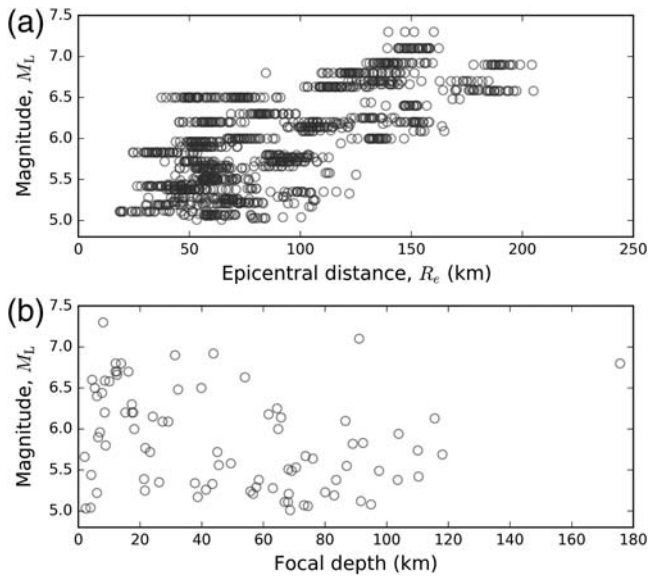


Figure 4. The distribution of M_L versus (a) the epicentral distance and (b) the focal depth.

the background noise. The amplitude spectral ratio of w_2 over w_1 at 23 Hz is ~ 3 , which is defined as signal-to-noise ratio (SNR). In our cautious picking of the P and S arrival and the inspection of time window w_1 and w_2 , the time window w_2 can contain the main energy of S wave for most of the events to estimate the κ_r value for each single record.

The second step is to determine the frequency windows and obtain the κ_r value automatically by moving windows. Equation (1) performs a linear relationship between the frequencies and spectral amplitudes, and describes a negative correlation indicating that the spectral amplitudes decrease with frequencies. To reduce the deviation of measuring the κ_r values, we apply the parameter of correlation coefficient under the process of the linear fit. The correlation coefficient R is one of the measures for goodness of fit describing the discrepancy between two variables, and the value is expected to be in the range of -1.0 and 1.0 . An example shown in Figure 6 is the amplitude spectra for both of the horizontal components. As mentioned earlier, the f_e should be above the f_c , which depends on the seismic moment and stress drop of the seismic source (Aki, 1967; Brune, 1970). The regional-dependent relationship between seismic moment (M_0) and the f_c was proposed by Huang and Wang (2009), in which they analyzed 22 aftershocks with $5.1 \leq M_L \leq 6.5$ of the 1999 Chi-Chi, Taiwan, earthquake (M_L 7.3). They concluded that the scaling law between M_0 and f_c is $\log(M_0) = -3.65 \times \log(f_c) + 23.36$. Wu *et al.* (2001) formulated the relationship between M_L and M_w from 32 events in the Taiwan area as $M_L = 4.53 \times \ln(M_w) - 2.09$ for $5.0 \leq M_L \leq 7.1$ and $4.8 \leq M_w \leq 7.6$, in which M_w is the moment magnitude. Substituting the minimum M_L 5.0 gives M_w 4.8. The M_0 can be calculated from M_w and is equal to 1.88×10^{16} N·m (Hanks and Kanamori, 1979). The f_c is 1.05 Hz according to the M_0 - f_c relation-

ship with a few extrapolations. Meanwhile, the dominant frequency of resonance effect is about 1.0 Hz due to sediments in the Taipei basin based on the method of amplitude spectrum ratio (Wen and Peng, 1998). The dominant frequencies determined by the horizontal-to-vertical (H/V) spectral ratio at a site from microtremor array surveyed in the Taipei basin are in the 0.5–5.0 Hz range (Huang, 2009). To reduce the effects of f_c and dominant frequency of resonance effect on measuring the κ_r value, we select $f_1 (= f_e)$ at 5, 6, 7, 8, 9, and 10 Hz, and the f_2 varies from 20 to 50 Hz with an increase of 1 Hz for iterations. In addition, the iteration will select the κ_r with the best correlation coefficient and $\text{SNR} \geq 3$. As shown in Figure 6b, the solid lines in the deepened gray colors with leading notes, that is, $f_1 = 5, 6, 7, 8, 9$, and 10, show that the correlation coefficients vary with frequencies. The best fit with $R = -0.87$ (denoted by an open square) is to select $f_1 = 5$ Hz and $f_2 = 23$ Hz for this recording. Meanwhile, the measured κ_r values also display for the condition of $f_1 = 5$ Hz and different f_2 from 20 to 50 Hz range. The dashed lines shown in Figure 5c,d are the fitting results.

Results

Figure 7 shows that the κ_r values of the two horizontal components increase gradually with R_e . We continue to compute $\kappa(r)$'s according to the site conditions and the focal depths. The site classification based on V_{S30} was constructed by the National Center for Research on Earthquake Engineering and the CWB in Taiwan to perform well loggings in 2000 for the engineering applications. The majority of the boreholes have a drilling depth of ~ 30 m. The United States' criteria for classifying sites following the NEHRP's provisions are based on the following shear velocities: $V_{S30} > 1500$ m/s for class A sites, $V_{S30} = 760$ – 1500 m/s for class B sites, $V_{S30} = 360$ – 760 m/s for class C sites, $V_{S30} = 180$ – 360 m/s for class D sites, and $V_{S30} < 180$ m/s for class E sites. In the Taipei area, 54 stations have site classifications based on the evaluation of V_{S30} (Kuo *et al.*, 2011, 2012), which are listed in Table 1. The κ_r - R_e couples are classified into four categories according to site conditions (Kuo *et al.*, 2011, 2012). In addition, datasets from the four site conditions are separated into two groups: crustal and subduction events, according to the focal depth of 40 km (Ustaszewski *et al.*, 2012). The class B, C, D, and E sites are shown in Figure 7a, 7b, 7c, and 7d, respectively. As shown in Figure 7, the solid circles denote data from crustal events, whereas the open circles denote those from subduction events. The increasing trend of fitting lines is displayed by a solid line and a dashed line, respectively, representing the crustal events and subduction events. The least-squared technique of robust linear model (RLM) is utilized to obtain the linear fitting instead of the commonly used method, ordinary linear fitting. The advantage of RLM is demonstrated in the study by Ktenidou *et al.* (2013). Ordinary linear fitting would

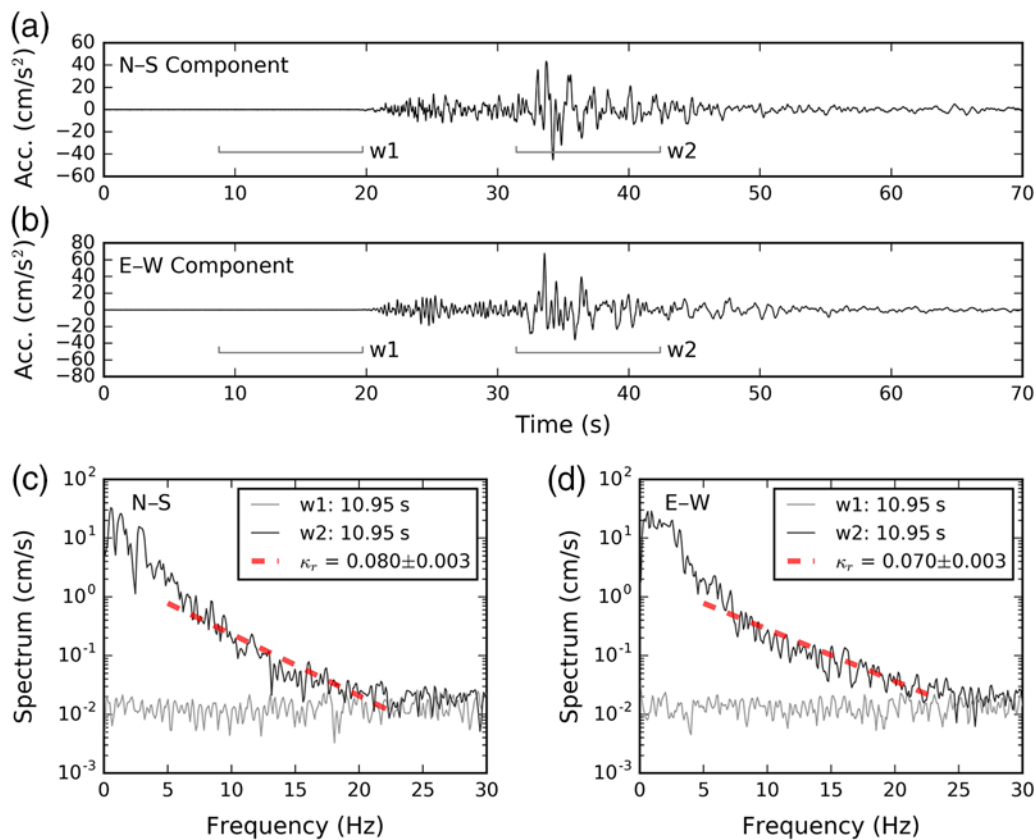


Figure 5. The waveform and spectral amplitudes for the north–south (N–S) component in (a) and (c), and those for the east–west (E–W) component in (b) and (d). The gray lines show the pre- P - and S -wave windows regarding $w1$ and $w2$ in (a) and (b). The dashed line depicts the least-squared fitting result. The color version of this figure is available only in the electronic edition.

have been influenced easily by the outliers in the data, which is not the case for RLM.

We observe that the slopes of crustal events are larger than those of subduction events for the four site classes. Similar results are also found in data from Japan (Van Houtte *et al.*, 2011) and Greece (Ktenidou *et al.*, 2013). The slopes of four site classes vary from 0.00010 to 0.00022 s/km for the crustal event, whereas the slopes are in the 0.000061–0.00015 s/km range for the subduction events. The slope (m) is considered as the regional effect of seismic-wave lateral propagation. Then, the site-specific κ_0 value can be calculated by minimizing the errors by applying the regional effect of m , accordingly, provided by the four site classes and the crustal and subduction events for each of the stations and following the equation $\kappa_r = \kappa_0 + m \times R_e$. The estimated κ_0 values for the 54 stations are also listed in Table 1.

Site-Specific κ_0 versus V_{S30}

The numbers of class B, C, D, and E sites are 3, 14, 32, and 5, respectively. Figure 8 shows the 54 couples of κ_0 and V_{S30} denoted by circles with one standard deviation bars. The dotted lines are the thresholds for the site classifications (i.e., class B, C, D, and E sites with notations at the bottom). The

κ_0 – V_{S30} couples perform a slightly decreasing κ_0 with increasing V_{S30} . The existing relations between κ_0 and V_{S30} provided by Silva *et al.* (1998), Chandler *et al.* (2006), Edwards *et al.* (2011), Van Houtte *et al.* (2011), and Ktenidou *et al.* (2015) from worldwide data are displayed by the thin dashed, the thin solid, the dashed-dotted, the thick dashed, and the thick solid lines, respectively. Silva *et al.* (1998) first introduced the relation using data for V_{S30} greater than 300 m/s in California. Chandler *et al.* (2006) provided the relationship in eastern North America for V_{S30} in the range of about 300–3000 m/s, for which the site conditions belong to class A, B, and C sites. Edwards *et al.* (2011) developed the relationships in Switzerland for class A, B, and C sites, namely V_{S30} greater than 400 m/s. Van Houtte *et al.* (2011) compiled the various results from the United States, Taiwan, France, and Switzerland to construct the κ_0 – V_{S30} relation for V_{S30} greater than 500 m/s. Ktenidou *et al.* (2015) provided the κ_0 – V_{S30} relation from a downhole array in Greece for V_{S30} greater than 180 m/s. These three relationships state that κ_0 decreases with increasing V_{S30} in different degrees of inclination, in which the relationships of Silva *et al.* (1998), Chandler *et al.* (2006), and Van Houtte *et al.* (2011) describe a larger inclination than those of Edwards *et al.* (2011) and Ktenidou *et al.* (2015). The discrepancies among these relationships diminish with increasing V_{S30} for the hard rock and the rock sites. The κ_0 – V_{S30} couples

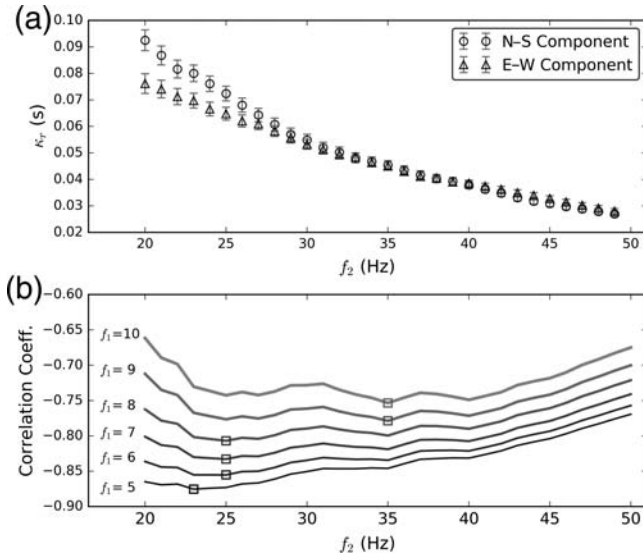


Figure 6. The spectral amplitudes for the N–S component and those for the E–W component. (a) The measured κ_r 's vary with f_2 by setting $f_1 = 5$ Hz and (b) the correlation coefficient versus different frequency bands. The squares show the lowest correlation coefficient for each of the pairs f_1 and f_2 .

show that κ_0 is independent of V_{S30} , which differ from the existing κ_0 – V_{S30} relationships, and imply the inadequacy of V_{S30} as a proxy for site attenuation in this area. Boore (2003) provided a useful way to estimate the averaged effective quality factor Q_{ef} within a sedimentary layer from site conditions of classes B and C. The value of Q_{ef} is assumed to be independent of frequency, which is supported by the evidences provided in Anderson and Hough (1984). The formula can be expressed as follows:

$$\kappa_0 = H/Q_{\text{ef}} \times V_S^{-1}, \quad (2)$$

in which H is the thickness and V_S is the averaged S -wave velocity. κ_0 is inversely proportional to Q_{ef} for the specific H and V_S . In the frequency range of 2.0–6.0 Hz, Wang (1993) obtained $Q = 126$, for the S waves in northern Taiwan. Fletcher and Wen (2005) investigate the Q -value of the coda wave, Q_c , within a narrow frequency band of 0.67–1.0 Hz in the Taipei basin and surrounding area from the records of the 1999 Chichi earthquake in Taiwan. The Q_c 's vary from 29 to 324. Using the spectral ratio method, Wen *et al.* (2004) calculate the Q -value of the shallow structure to a depth of ~ 140 m from a downhole array in Taipei basin. A time window after the S -wave arrival for computation is 10 s, indicating the minimum analytic frequency to be 0.1 Hz. Four Q models as functions of frequency are proposed in various depths as follows: $Q(f) = 3.6f^{0.96}$ for a 0–30 m depth; $Q(f) = 7.2f^{0.99}$ for a 30–60 m depth; $Q(f) = 10.2f^{1.17}$ for a 60–90 m depth; and $Q(f) = 40.7f^{1.24}$ for a 90–141 m depth. The average Q -values are 32.5, 70.2, 156.4, and 745.8 when computing the four Q models in the frequency band at 0.1–20.0 Hz. Despite their suitable use of frequency, Q in-

creases with diminishing depths/areas. The high Q results in the low κ_0 . It is suggested that the Q for depth greater than 30 m affects the κ_0 . Many sites with low V_{S30} located inside the basin display a similar κ_0 to those with high V_{S30} . Furthermore, Ktenidou *et al.* (2014) compiled the existing κ_0 – V_{S30} couples and questioned if V_{S30} represented the attenuation of κ_0 due to the effect of regional Q . They also suggest that κ_0 correlates with the deeper structure as well; that is, thickness of sediment above the base. The thickness of the sediment and dominant/resonant frequency overlying the Tertiary base against κ_0 will be investigated in [The Effective \$Q\$ for the Alluvial Sediment](#) and [The Correlation between \$\kappa_0\$ and the Dominant/Resonant Frequency in the Basin](#) sections. Besides, the κ_0 values of class B sites maintain an average of ~ 0.05 s because of stabilization, which is meant to be a limited effect of hysteretic damping, nonlinearity, and scattering in softened sediment (Ktenidou *et al.*, 2015).

The Effective Q for the Alluvial Sediment

One of the aforementioned issues involves correlating κ_0 with the layer thickness to the base rock (Tertiary base rock with V_S is ~ 1500 m/s). Wang *et al.* (2004) utilize the seismic reflections and then integrate several sets of borehole data to develop an image of the subsurface tomography of sediments underneath the Taipei basin. Herein, we calculate the thickness (in meters) to Tertiary base (D_B), according to the subsurface tomographic data for 28 stations, which belong to class C, D, and E sites, as listed in Table 1.

As shown in Figure 9, the κ_0 values increase mildly with D_B . The open circles with one standard deviation denote the κ_0 – D_B couples, which mostly distribute with D_B less than 350 m. We attempt to depict the tendency according to a linear fit of the data with $D_B < 350$ m. The slope (m_{D_B}) and intercept (y_{D_B}) of a linear fit are 0.000025 s/m and 0.050 s, respectively. The standard deviations of m_{D_B} and y_{D_B} are 0.000020 s/m and 0.003 s. We observe that $y_{D_B} = 0.050$ s is close to κ_0 of the three class B sites (i.e., TAP067, TAP071, and TAP086, namely 0.050, 0.049, and 0.050 s, respectively). These class B sites are located outside the basin. The increasing trend of κ_0 against D_B agrees with the results of Campbell (2009) in North America and Ktenidou *et al.* (2015) in northern Greece. The two estimates provided by Campbell (2009) that include site classes B and C (table 2 and equations 22 and 23 in his study) are displayed, respectively, by a gray solid and a dashed-dotted lines. The κ_0 – D_B couples distribute greatly above the estimates of Campbell (2009) because of the site classes in use. Furthermore, the dashed line shows the tendency of Ktenidou *et al.* (2015) from a downhole array, in which V_S 's are greater than 180 m/s.

Solving Q_{ef} from equation (2), the results can be $Q_{\text{ef}} = (H/\kappa_0) \times V_S^{-1}$. Campbell (2009) gives the expression, following the approaches of Hough and Anderson (1988) and Liu *et al.* (1994), for interpreting the sediments as a uniform layer over a half-space to be $Q_{\text{ef}} = (b^{-1}) \times V_S^{-1}$, in which b is the slope of the relationship between κ_0 and H .

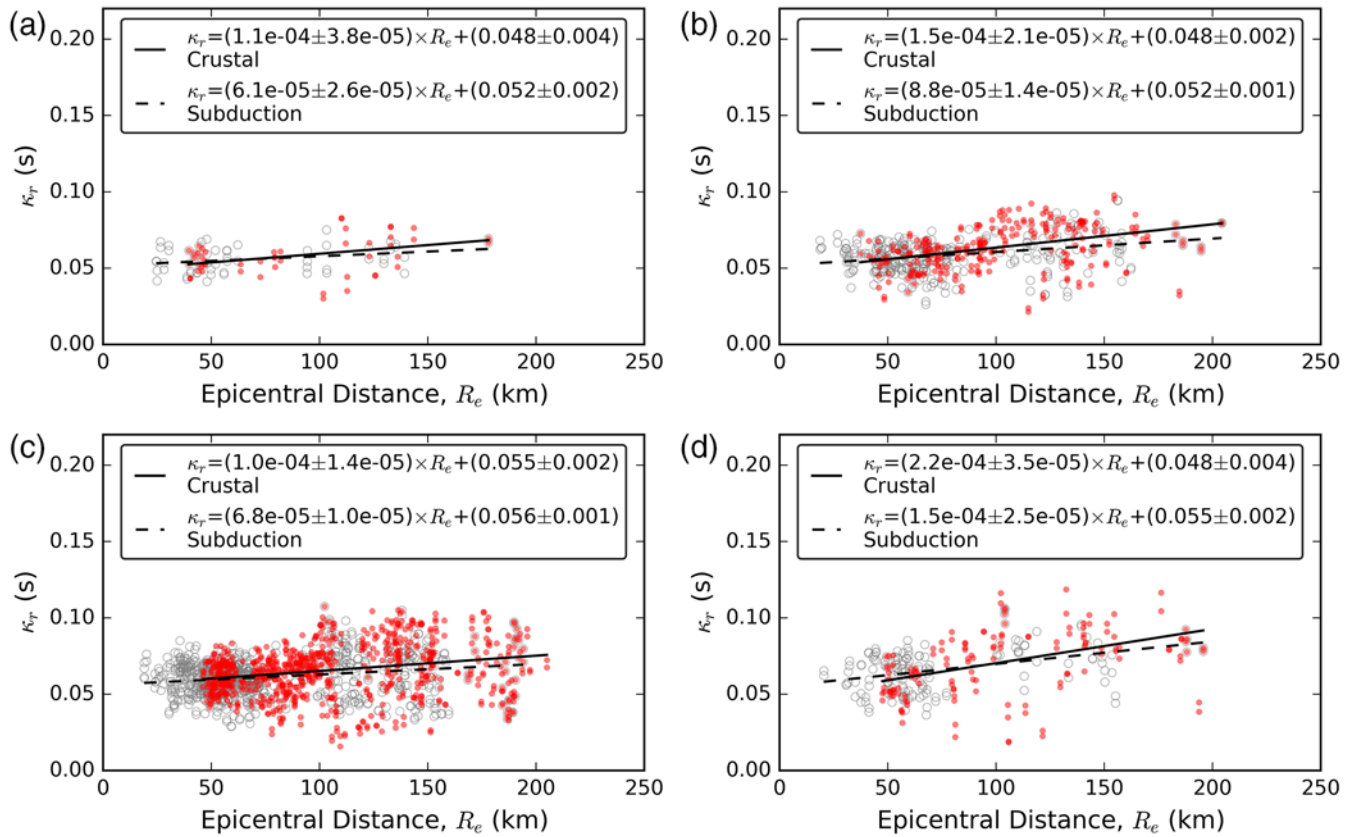


Figure 7. The measured κ values of the two horizontal components versus the epicentral distance. The solid circles represent the data from the crustal event, and open circles in gray are from the subduction event. The κ values are grouped accordingly by the site classification from Kuo *et al.* (2012) into (a) class B site, (b) class C site, (c) class D site, and (d) class E site. The color version of this figure is available only in the electronic edition.

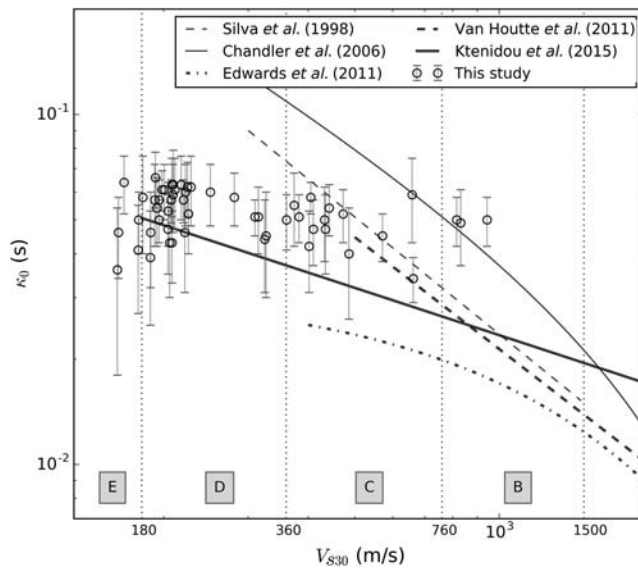


Figure 8. The relations between κ_0 and V_{S30} for the site condition of class B, C, D, and E sites, as well as those of the global relationship from five studies for comparison.

Ktenidou *et al.* (2015) give a similar concept after Hough and Anderson (1988) in terms of $\kappa_{0\text{sur}} = \kappa_{0\text{DH}} + t^*$, in which $\kappa_{0\text{sur}}$ and $\kappa_{0\text{DH}}$ are the measured κ_0 , respectively, at the surface and downhole, and t^* as the attenuation of the layer in between. In their model, t^* is computed and integrated using horizontal stratified layers (i) with parameters, such as thickness (H_i), V_{si} , and Q_i by following the equation $t^* = H_i / (V_{si} \times Q_i)$. Herein, we assume a single geological layer with various thicknesses as a representative of the sediment overlying the Tertiary base rock. The effects regarding scattering and nonlinearity from the sediment are excluded from the sediment. Therefore, the equation can be rewritten as $Q = (H/t^*) \times V_S^{-1}$, in which Q can be considered as Q_{ef} and H/t^* denotes the aforementioned b^{-1} .

The H -values can correspond to D_B 's in this study. Table 2 lists the V_S structure of the four sedimentary layers underneath the Taipei basin. The thickness of the sediment varies increasingly from the NW part to the SE part. The averaged V_S values are calculated by the thickness of the layer divided by the travel time, under the assumption that the seismic wave propagates vertically through the layer, and are listed in the last column of Table 2. An average shear-wave velocity \tilde{V}_S is 530.9 m/s. Substituting the \tilde{V}_S ($= 530.9$ m/s) and m_{D_B} ($= 0.000025$ s/m) for $Q_{\text{ef}}(z)$, a computed result

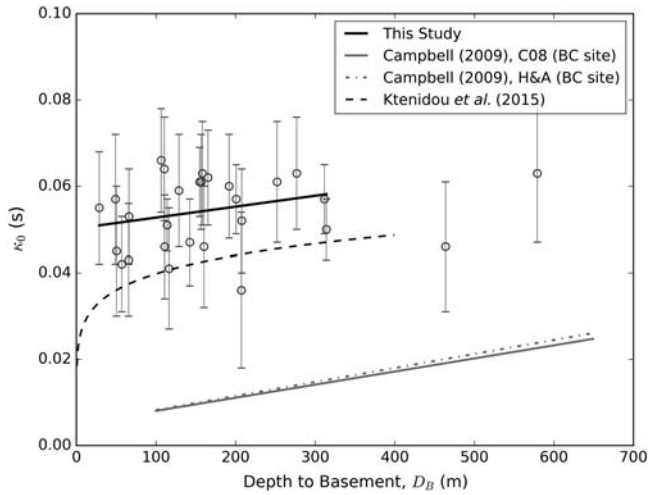


Figure 9. The relation between the estimated κ_0 values and the depth to the Tertiary base rock.

gives 75.3. Furthermore, given plus and minus one standard deviation on m_{D_B} , namely 0.000045 and 0.000005 s/m, results in two values of Q_{ef} as 41.9 and 376.7. The calculated Q_{ef} values fall in reasonable ranges compared with the aforementioned estimation of Wang (1993), Wen *et al.* (2004), and Fletcher and Wen (2005), despite their suitable use of frequency. We suggest that Q_{ef} can represent ground-motion simulation in the Taipei basin.

The Correlation between κ_0 and the Dominant/Resonant Frequency in the Basin

We proceed to correlate the κ_0 with the dominant/resonant frequency (hereafter denoted as f_r) in the Taipei basin at 28 locations (Huang, 2009). The f_r values are measured using the microtremor array installed in the Taipei basin according to the technique of the H/V spectral ratios (Nakamura, 1989). The $f_r (= V_S/4H)$ indicate where the amplitude spectral ratios are largest and are greatly correlated with the thickness of sediment above the base rock. Figure 10 shows that κ_0 varies with f_r . The open circles with one standard deviation bar display the κ_0 - f_r couples. The f_r values range from 0.21 to 0.99 Hz, whereas the κ_0 values vary from

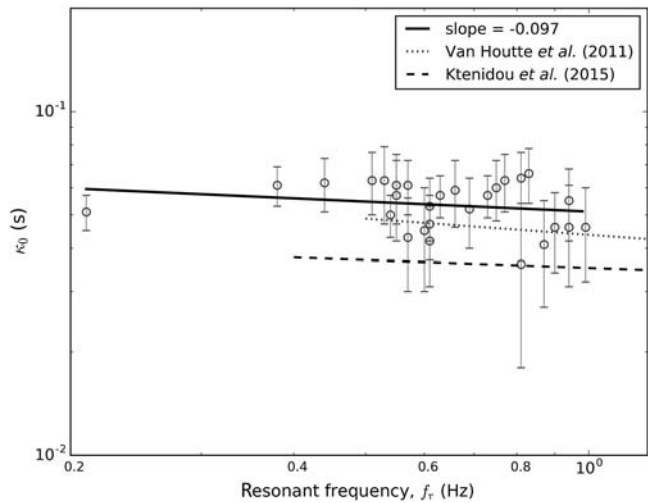


Figure 10. The relation between the estimated κ_0 values and the resonant frequency independently obtained from horizontal to vertical spectral ratios of microtremor array surveyed in the Taipei basin.

0.036 to 0.066 s. The black line displays the least-squared fitting of both logarithmic axes given a slope of -0.097 , which implies a slight correlation between κ_0 and f_r . Additionally, the similar tendency of Van Houtte *et al.* (2011) and Ktenidou *et al.* (2015) are depicted by a dotted line and a dashed line, respectively.

Conclusion

The high-frequency decay parameter κ_r measured from the semilogarithmic amplitude spectra of the S wave is determined automatically by moving frequency windows. We apply varied frequency windows in the 5–10 Hz range at the start and 20–50 Hz when stopping. Each calculation routine for the least-squared fitting can obtain a correlation coefficient over a frequency window of more than 10 Hz (10–20 Hz). The κ_r values are determined by the best correlation coefficient. The site-specific κ_0 values at 54 stations are computed using the anelastic effect of regional geological structure by grouping data into crustal and subduction events according to the focal depth and site classification (i.e., class B, C, D, and E sites). κ_0 's are in the 0.034–0.066 s range. The anelastic effects are larger for the crustal events than for the subduction events. The κ_0 values are compared with the V_{S30} , displaying an independency of V_{S30} on κ_0 and implying the inadequacy of V_{S30} as a proxy for site attenuation in this area. Notably, κ_0 is ~ 0.05 s for the rock site because of stabilization. The relationships of the κ_0 - D_B couples provide a useful method for estimating the Q_{ef} value in a sedimentary layer with averaged V_S . According to the estimate of methodology, Q_{ef} is 75.3 for the whole sedimentary layer (above the Tertiary base). Given one standard deviation on the relationships of the κ_0 - D_B couples, the resultant Q_{ef} values are in the 41.9–376.7 range. Finally, the κ_0 values are also compared with the dominant/resonant frequency regarding the thickness of a sediment above the base rock. A mildly decreasing trend in κ_0 with

Table 2

S-Velocity for the Four Sedimentary Layers underneath the Taipei Basin and the Inferred Q_{ef} for the Sungshan Formation and the Whole Sediment

| | D_{NW} (m) | D_{SE} (m) | V_S (m/s) | \bar{V}_S (m/s) | Q_{ef} |
|----------|--------------|--------------|-------------|-------------------|-------------------|
| Sungshan | 0–20 | 0–15 | 170 | | |
| | 20–50 | 15–35 | 230 | | |
| | 50–100 | 35–50 | 340 | | |
| Chingmei | 100–160 | 50–100 | 450 | | |
| Wuku | 160–320 | 100–200 | 600 | | |
| Banchiao | 320–700 | 200–300 | 880 | 530.9 | 75.3 (41.9–376.7) |

D_{NW} , D_{SE} , V_S after Wang *et al.* (2004) representing the depth of the northwest (NW), depth of the southeast (SE), and the S velocity, respectively.

increasing dominant/resonant frequency can be observed. The tendency indicates that κ_0 correlates with the several hundred meters beneath the site.

Data and Resources

The seismic events and records used in this study are available at <http://gdms.cwb.gov.tw/> (last accessed January 2014), which are a part of the database managed by the Central Weather Bureau of Taiwan.

Acknowledgments

The authors thank the Central Weather Bureau, Taiwan, for providing high-quality earthquake data. This study was sponsored by National Science and Technology Center for Disaster Reduction and the Ministry of Science and Technology (under Grant Number MOST 104-2116-M-865-001). The authors give thanks to Associate Editor Hiroshi Kawase and two anonymous reviewers for their valuable comments on this article.

References

- Aki, K. (1967). Scaling law of seismic spectrum, *J. Geophys. Res.* **72**, 1217–1231.
- Anderson, J. G. (1991). A preliminary descriptive model for the distance dependence of the spectral decay parameter in southern California, *Bull. Seismol. Soc. Am.* **81**, 2186–2193.
- Anderson, J. G., and S. E. Hough (1984). A model for the shape of the Fourier amplitude spectrum of acceleration at high frequencies, *Bull. Seismol. Soc. Am.* **74**, 1969–1993.
- Boore, D. M. (1983). Stochastic simulation of high-frequency ground motions based on seismological models of the radiated spectra, *Bull. Seismol. Soc. Am.* **73**, 1865–1894.
- Boore, D. M. (1996). SMSIM-Fortran programs for simulating ground motions from earthquakes: Version 1.0, *U.S. Geol. Surv. Open-File Rept. 96-80-A, 96-80-B*, 69 pp.
- Boore, D. M. (2003). Prediction of ground motion using the stochastic method, *Pure Appl. Geophys.* **160**, 635–676.
- Boore, D. M. (2004). Estimating $V_s(30)$ (or NEHRP site classes) from shallow velocity models (depths < 30 m), *Bull. Seismol. Soc. Am.* **94**, no. 2, 591–597.
- Boore, D. M., and W. B. Joyner (1997). Site amplifications for generic rock sites, *Bull. Seismol. Soc. Am.* **87**, 327–341.
- Brune, J. N. (1970). Tectonic stress and the spectra of seismic shear waves from earthquakes, *J. Geophys. Res.* **75**, 4997–5009.
- Building Seismic Safety Council (BSSC) (2001). *NEHRP Recommended Provisions for Seismic Regulations for New Buildings and other Structures, Part 1: Provisions*, Federal Emergency Management Agency (Report FEMA 368) (2000 Edition), Washington, D.C.
- Campbell, K. W. (2009). Estimates of shear-wave Q and κ_0 for unconsolidated and semiconsolidated sediments in eastern North America, *Bull. Seismol. Soc. Am.* **99**, 2365–2392.
- Chandler, A. M., N. T. K. Lam, and H. H. Tsang (2006). Near-surface attenuation modelling based on rock shear-wave velocity profile, *Soil Dynam. Earthq. Eng.* **26**, 1004–1014.
- Edwards, B., D. Fäh, and D. Giardini (2011). Attenuation of seismic shear wave energy in Switzerland, *Geophys. J. Int.* **185**, 967–984.
- Edwards, B., O. J. Ktenidou, F. Cotton, N. Abrahamson, C. Van Houtte, and D. Fäh (2015). Epistemic uncertainty and limitations of the κ_0 model for near-surface attenuation at hard rock sites, *Geophys. J. Int.* **202**, 1627–1645.
- Fletcher, J. B., and K. L. Wen (2005). Strong ground motion in the Taipei basin from the 1999 Chi-Chi, Taiwan, earthquake, *Bull. Seismol. Soc. Am.* **95**, 1428–1446.
- Hanks, T. C., and H. Kanamori (1979). A moment magnitude scale, *J. Geophys. Res.* **84**, 2348–2350.
- Holzer, T. L., A. C. Padovani, M. J. Bennett, T. E. Noce, and J. C. Tinsley (2005). Mapping NEHRP V_{S30} site classes, *Earthq. Spectra* **21**, 353–370.
- Hough, S. E., and J. G. Anderson (1988). High-frequency spectra observed at Anza, California: Implications of Q structure, *Bull. Seismol. Soc. Am.* **78**, 692–707.
- Huang, J. Y. (2009). Using microtremor measurement to study the site effect in Taiwan area, *Master's Thesis*, National Central University, Taoyuan City, Taiwan, 240 pp. (in Chinese with English abstract).
- Huang, M. W., and J. H. Wang (2009). Scaled energies of $M_L \geq 5.1$ after-shocks of the 1999 Chi-Chi, Taiwan, earthquake measured from local seismograms, *Terr. Atmos. Ocean. Sci.* **20**, no. 5, 671–685.
- Huang, M. W., J. H. Wang, H. H. Hsieh, K. L. Wen, and K. F. Ma (2005). Frequency-dependent sites amplifications evaluated from well-logging data in central Taiwan, *Geophys. Res. Lett.* **32**, L21302, doi: [10.1029/2005GL023527](https://doi.org/10.1029/2005GL023527).
- Huang, M. W., J. H. Wang, H. H. Hsieh, K. L. Wen, K. F. Ma, and K. C. Chen (2009). High frequency site amplification evaluated from borehole data in the Taipei basin, *J. Seismol.* **13**, 601–611.
- Huang, M. W., J. H. Wang, K. F. Ma, C. Y. Wang, J. H. Hung, and K. L. Wen (2007). Frequency-dependent site amplifications with $f \geq 0.01$ Hz evaluated from the velocity and density models in Central Taiwan, *Bull. Seismol. Soc. Am.* **97**, 624–637.
- Ktenidou, O.-J., N. A. Abrahamson, S. Drouet, and F. Cotton (2015). Understanding the physics of kappa (κ): Insights from a downhole array, *Geophys. J. Int.* **203**, 678–691, doi: [10.1093/gji/ggv315](https://doi.org/10.1093/gji/ggv315).
- Ktenidou, O.-J., F. Cotton, N. A. Abrahamson, and J. G. Anderson (2014). Taxonomy of kappa: A review of definitions and estimation approaches targeted to applications, *Seismol. Res. Lett.* **85**, 135–146.
- Ktenidou, O.-J., C. Gélis, and L.-F. Bonilla (2013). A study on the variability of kappa (κ) in a borehole: Implications of the computation process, *Bull. Seismol. Soc. Am.* **103**, 1048–1068.
- Kuo, C. H., K. L. Wen, H. H. Hsieh, T. M. Chang, C. M. Lin, and C. T. Chen (2011). Evaluating empirical regression equations for V_S and estimating V_{S30} in northeastern Taiwan, *Soil Dynam. Earthq. Eng.* **31**, 431–439.
- Kuo, C. H., K. L. Wen, H. H. Hsieh, C. M. Lin, and T. M. Chang (2012). Site classification of free-field TSMIP stations using the logging data of EGDT, *Eng. Geol.* **129–130**, 68–75.
- Lee, S. J., H. W. Chen, Q. Liu, D. Komatitsch, B. S. Huang, and J. Tromp (2008). Three-dimensional simulations of seismic-wave propagation in the Taipei basin with realistic topography based upon the spectral-element method, *Bull. Seismol. Soc. Am.* **98**, 253–264.
- Lee, Y. T., K. F. Ma, Y. J. Wang, and K. L. Wen (2015). An empirical equation of effective shaking duration for moderate to large earthquakes, *Nat. Hazards* **75**, 1779–1793.
- Liu, K. S., T. C. Shin, and Y. B. Tsai (1999). A free-field strong motion network in Taiwan: TSMIP, *Terr. Atmos. Ocean. Sci.* **10**, 377–396.
- Liu, Z., M. E. Wuenschel, and R. B. Herrmann (1994). Attenuation of body waves in the central New Madrid seismic zone, *Bull. Seismol. Soc. Am.* **84**, 1112–1122.
- Miksat, J., K. L. Wen, F. Wenzel, V. Sokolov, and C. T. Chen (2010). Numerical modelling of ground motion in the Taipei basin: Basin and source effects, *Geophys. J. Int.* **183**, 1633–1647.
- Nakamura, Y. (1989). A method for dynamic characteristics estimation of subsurface using microtremor on the ground surface, *Q. Rep. Railway Tech. Res. Inst.* **30**, 25–30.
- Papageorgiou, A. S., and K. Aki (1983). A specific barrier model for the quantitative description of inhomogeneous faulting and the prediction of strong ground motion, *Bull. Seismol. Soc. Am.* **73**, 693–722.
- Parolai, S., and D. Bindi (2004). Influence of soil-layer properties on k evaluation, *Bull. Seismol. Soc. Am.* **94**, 349–356.
- Purvance, M. D., and J. G. Anderson (2003). A comprehensive study of the observed spectral decay in strong-ground accelerations records in Guerrero, Mexico, *Bull. Seismol. Soc. Am.* **93**, 600–611.
- Scherbaum, F., F. Cotton, and H. Staedteke (2006). The estimation of minimum misfit stochastic models from empirical ground-motion equations, *Bull. Seismol. Soc. Am.* **96**, 427–445.

- Shin, T. C. (1993). The calculation of local magnitude from the simulated Wood–Anderson seismograms of the short-period seismograms, *Terr. Atmos. Ocean. Sci.* **4**, 155–170.
- Shin, T. C., C. H. Chang, H. C. Pu, H. W. Lin, and P. L. Leu (2013). The Geophysical Database Management System in Taiwan, *Terr. Atmos. Ocean. Sci.* **24**, 11–18.
- Silva, W., R. Darragh, N. Gregor, G. Martin, N. Abrahamson, and C. Kircher (1998). Reassessment of site coefficients and near-fault factors for building code provisions, *Tech. Rept. Program Element II: 98-HQGR-1010*, Pacific Engineering and Analysis, El Cerrito, California.
- Sokolov, V., K. L. Wen, J. Miksat, F. Wenzel, and C. T. Chen (2009). Analysis of Taipei basin response for earthquakes of various depths and locations using empirical data, *Terr. Atmos. Ocean. Sci.* **20**, 687–702.
- Sokolov, V. Y., C. H. Loh, and K. L. Wen (2004). Evaluation of generalized site response functions for typical soil classes (B, C, and D) in Taiwan, *Earthq. Spectra* **20**, 1279–1316.
- Ustaszewski, K., Y. M. Wu, J. Suppe, H. H. Huang, C. H. Chang, and S. Carena (2012). Crust-mantle boundaries in the Taiwan-Luzon arc-continent collision system determined from local earthquake tomography and 1D models: Implications for the mode of subduction polarity reversal, *Tectonophysics* **578**, 31–49.
- Van Houtte, C., S. Drouet, and F. Cotton (2011). Analysis of the origins of κ (κ) to compute hard rock to rock adjustment factors for GMPEs, *Bull. Seismol. Soc. Am.* **101**, 2926–2941.
- Wang, C. Y., Y. H. Lee, and H. C. Chang (1996). P- and S-wave velocity structures of the Taipei basin, *Symposium on Taiwan Strong Motion Instrument Program (II)*, Central Weather Bureau, 171–177.
- Wang, C. Y., Y. H. Lee, M. L. Ger, and Y. L. Chen (2004). Investigating subsurface structures and P- and S-wave velocities in the Taipei basin, *Terr. Atmos. Ocean. Sci.* **15**, 609–627.
- Wang, J. H. (1993). Q values of Taiwan: A review, *J. Geol. Soc. China* **36**, 15–24.
- Wen, K. L., and H. Y. Peng (1998). Site effect analysis in the Taipei basin: Results from TSMIP network data, *Terr. Atmos. Ocean. Sci.* **9**, 691–704.
- Wen, K. L., T. M. Chang, H. J. Chiang, and C. M. Lin (2004). Ground motion responses in the Taipei urban area, *Proc. of International Workshop on Strong Ground Motion Prediction and Earthquake Tectonics in Urban Areas*, 7 pp.
- Wen, K. L., L. Y. Fei, H. Y. Peng, and C. C. Liu (1995). Site effect analysis from the records of the Wuku downhole array, *Terr. Atmos. Ocean. Sci.* **6**, no. 2, 285–298.
- Wu, Y. M., T. C. Shin, and C. H. Chang (2001). Near real-time mapping of peak ground acceleration and peak ground velocity following a strong earthquake, *Bull. Seismol. Soc. Am.* **95**, 1218–1228.
- National Science and Technology Center for Disaster Reduction
9F, No.200, Section 3, Beisin Road, Xindian District
New Taipei City 23143, Taiwan
mwhuang@ncdr.nat.gov.tw
(M.-W.H., C.-L.C., S.-Y.L.)
- Department of Earth Sciences
National Central University
No. 300, Zhongda Road, Zhongli District
Taoyuan City 32001, Taiwan
(K.-L.W.)
- Institute of Geophysics
National Central University
No. 300, Zhongda Road, Zhongli District
Taoyuan City 32001, Taiwan
(S.-C.C.)
- Eastern Taiwan Earthquake Research Center
No. 1, Section 2, Da Hsueh Road, Shoufeng
Hualien 97401, Taiwan
(K.-P.C.)

Manuscript received 4 March 2016;
Published Online 2 May 2017